Radiological characterization of large electromagnets in view of their elimination as very low-level wastes

Thomas Frosio *, Matteo Magistris, Nabil Menaa, Régis Michaud, Maeva Rimlinger, Chris Theis

Radiation Protection Group, European Organization for Nuclear Research, 1211, Geneva 23, Switzerland

ARTICLE INFO

ABSTRACT

The operation of particle accelerators at CERN requires the use of electromagnets, which are accelerator components used to guide and focus charged particles. In the framework of maintenance activities and machine upgrades or dismantling, a large number of magnets are removed from the accelerator complex and required characterization in view of their disposal as radioactive waste. The present document describes a new characterization methodology, which is applied to radioactive magnets with masses up to 25 tons and lengths up to 6 meters. The characterization of such large electromagnets is challenging due to their heterogeneous composition, variable radiological history, technical constraints related to handling, and the operational complexity of evaluating activity values with gamma spectroscopy . The innovative method proposed in this paper is based on the establishment of transfer functions which convert dose-rate to a radionuclide inventory. This method is validated by comparison with accurate gamma spectroscopy and benchmarking.

1. Introduction

The operation of particle accelerators at CERN requires the use of electromagnets, which are accelerator components used to guide and focus charged particles. In the framework of maintenance activities and machine upgrades or dismantling over the last 40 years, a large number of magnets were removed from the accelerator complex and require characterization in view of their disposal as radioactive waste.

The electromagnets can be very large, with a length of up to 6 meters and over 20 tons in mass. Their characterization is particularly challenging due to their heterogeneous composition, variable radiological history, technical constraints related to handling, and the operational complexity of evaluating activity values with gamma spectroscopy. In particular, destructive analyses are problematic, because workshops that are equipped for handling magnets may not be an adequate area for taking samples, which would involve creation of dust and radiological risks. The activity distribution is such, that the highest level of activity concentration are expected inside the magnets, in parts which are not easily accessible for measurement. Last but not least, each magnet has a different geometry and would require a dedicated calibration curve for gamma spectroscopy.

The innovative method proposed in this paper is based on the establishment of transfer functions which convert dose-rate to a radionuclide inventory. This method is validated by comparison with accurate gamma spectroscopy measurements.

In the first part of this document, we give an overview of the material to characterize. We then describe the calculations performed to obtain the list of expected radionuclides and their relative contribution to the total activity (also called "fingerprints"). Next, we establish transfer functions in order to normalize the fingerprints to measured levels of dose-rate. Finally, we validate our methodology by comparing high-performance gamma spectroscopy measurements with the results from the transfer functions.

2. Physical and chemical description of magnets

Electromagnets are made of three main parts: copper coils, an iron yoke and a steel supporting structure. For the purpose of characterization, the vacuum chamber – if present – is assimilated to the case of the supporting structure because it is made of steel. The magnets can possibly include other small parts like pieces of cables, plastic covers and piping, which in terms of mass can be considered as negligible with respect to the main constituents.

The radionuclide inventory is therefore established for the following metals: iron, stainless steel and copper. These metals are assigned a standard chemical composition, partly taken from the CERN catalog of materials [1] and partly from the literature, with a view to be representative of the main parts that constitute a magnet (Tables 1–3).

The exact chemical composition of these metals can vary depending on the specific magnet considered, and variations on the presence of trace elements can be found even among different parts of the same metal taken from the same magnet. However, in the general case such variations are likely to smooth out when averaged over the total mass

Table 1
Chemical composition of iron (ARMCO pure iron grade 4). Values are given as weight fractions (percentage).

	Fe	Mn	Cu	C	P	N	Co	Sn	S
Iron_ARMCO	99.887	0.06	0.03	0.01	0.005	0.005	0.005	0.005	0.003

Table 2
Chemical composition of stainless steel (304L). Values are given as weight fractions (percentage).

	C	Cr	Co	Fe	Mn	Ni	P	Si	S
Steel_304L	0.03	18.5	0.1	67.0825	2.0	11.25	0.0225	1.0	0.015

Table 3
Chemical composition of copper (OFE, with the addition of traces of silver [2,3]). Values are given as weight fractions (percentage).

	Cu	Ag	S	Bi	Pb	O	Cd	Hg	Zn
Copper_OFE	99.94	0.05	0.0018	0.001	0.001	0.0005	0.0001	0.0001	0.0001

of a batch of waste to be eliminated, which is typically in the order of hundreds of tons. In addition, a large fraction of radionuclides are produced via spallation reactions with high-energy secondary particles, for which trace elements play a minor role.

3. Radionuclide inventory and fingerprints

3.1. Analytical predictions

The calculation of induced radioactivity is performed with the analytical code ActiWiz version 2.9.8 [4], which is based on extensive Monte Carlo simulations carried out with the code FLUKA [5,6].

The calculations are carried out for two representative locations during irradiation, namely in case of activation occurring:

– within bulky materials surrounding the beam impact area;
– at 10 cm lateral distance to target.

The primary proton beam is assigned 4 different energies: 1.4 GeV, 14 GeV/c, 400 GeV/c and 7 TeV in order to cover the entire spectrum of proton machines at CERN with the exception of Linac4, which will require a separate study.

The irradiation time is set to 30 years – which on one hand is representative of the typical lifetime of a magnet and on the other hand will result in saturation activities for the most important radionuclides – whilst a whole range of possible waiting times is considered, from 3 to 40 years. More specifically, three groups of possible sets of waiting time are identified:

– from 3 to 10 years (8 scenarios: 3, 4, 5, . . . 10 years);
– from 10 to 20 years (11 scenarios);
– from 20 to 40 years (21 scenarios).

A total of 304 possible activation scenarios are studied with ActiWiz for each of the 3 material types considered (iron, stainless steel and copper). For each activation scenario, ActiWiz provides an exhaustive list of the radionuclides produced ("nuclide vector"), with their specific activity normalized to a beam loss of one particle per second, for a given irradiation scenario and material.

The final repository for very low-level waste managed by ANDRA (Agence Nationale pour la gestion des Déchets RAdioactifs) would only accept waste items with IRAS < 10.0, where IRAS (in French: "Indice Radiologique d'Acceptation en Stockage") is a quantity obtained by dividing the specific activity of a radionuclide by its corresponding activity limit set by ANDRA, and adding up all the contributions from the different radionuclides. In addition, the acceptance criteria of the repository only concerns radionuclides with an activity level above the

so-called "declaration limit"; any radionuclide with activity level below such limit can be simply disregarded for the purposes of radiological characterization. For a given radionuclide inventory produced with ActiWiz we therefore retain only those radionuclides whose activity level is above the declaration limit, once the entire inventory is normalized to IRAS = 10.0. The details of the IRAS calculations are described in Eq. (1).

Calculation of the IRAS for a waste item.

$$\forall a_i > DL_i, IRAS = \sum_i \frac{a_i}{10^{class i}} < 10 \tag{1}$$

In Eq. (1), a_i is the specific activity of the radionuclide i, $class i$ is the class of the radionuclide i (1, 2, 3, provided by ANDRA), corresponding to its radiotoxicity and DL_i is the declaration limit provided by ANDRA.

Once the radionuclides with activity below the declaration limit are discarded, we classify the remaining, relevant radionuclides as ETM (Easy-To-Measure) when they can be measured by gamma spectroscopy and DTM (Difficult-To-Measure) when they cannot be measured except with destructive analyses.

Table 4 provides a list of the radionuclides of interest, with their activity limits (to be used for the calculation of the IRAS) and declaration limits.

3.2. Expected levels of activity and fingerprints for a given material

The studies [7–11] recommend the use of gamma spectroscopy measurements to evaluate the activity of ETM radionuclides, and scaling factors (i.e., activity ratio between a given radionuclide and a reference gamma emitter) for DTM radionuclides. However, in the case of large electromagnets at CERN it is not technically feasible to perform extensive in-situ measurements of gamma spectroscopy for every magnet. We then decided to extend the concept of scaling factors also to ETM radionuclides and adopted the so-called "fingerprints", which is a list of both ETM and DTM radionuclides with their activity expressed as percentage of the total activity. By means of dose-to-activity transfer functions, the fingerprints are normalized to the average dose-rate measured in contact with the magnet in order to determine the absolute levels of activity, without resorting to gamma spectroscopy.

ActiWiz provides the nuclide vector of each activation scenario, with activity levels normalized to a beam loss of one particle per second. However, the nuclide vectors of different irradiation scenarios for the same material are not directly comparable, because beam losses are typically inversely proportional with the beam energy whilst the default beam loss in ActiWiz is constant.

In order to overcome this technical challenge, the average specific activity for the radionuclide i in the material m is calculated with a geometric mean following Eq. (2), where N is the total number of scenarios s considered, $aw_{i,s,m}$ is the specific activity calculated by ActiWiz for the scenario s, the material m and the radionuclide i under the assumption of one beam particle lost per second, E_s is the beam energy for the scenario s and $k = 6.2E18$ eV/s which corresponds to 1 W. Hence, dividing k by E_s gives the number of particles lost for 1 W of losses.. The beam loss of 1 W is used to normalize the different simulated scenarios at different primary particle energies in a comparable manner. It should be noted that the value of the constants k and E_s have no impact on the evaluation of the specific activity in a magnet, as they disappear during renormalization of the fingerprints to the measured level of dose-rate. Nevertheless, it does provide a first estimate of the expected levels of activity in a magnet irradiated under typical conditions. Table 5 provides an example of expected levels of activity in copper, steel and iron. The fingerprints can be obtained by converting expected levels of activity into fractions of total activity.

Calculation of average specific activity from the nuclide vector obtained with ActiWiz.

$$\bar{a}_{i,m} = \sqrt[N]{\prod_{s=1}^{N} {}^{k/E_s} aw_{i,s,m}} \tag{2}$$

Table 4
List of relevant radionuclides with activity limits and declaration limits.

	Activity limits (Bq/g)	Declaration limits (Bq/g)	Classification		Activity limits (Bq/g)	Declaration limits (Bq/g)	Classification
H-3	1000	1	DTM	Ti-44	10	0.1	ETM
C-14	1000	0.01	DTM	Mn-54	10	0.1	ETM
Na-22	10	0.1	ETM	Fe-55	1000	10	DTM
Cl-36	1000	0.01	DTM	Co-60	10	0.1	ETM
Ar-39	1000	10	DTM	Ni-63	1000	10	DTM
Ca-41	1000	0.01	DTM	Ag-108m	10	2.5E−4	ETM

Table 5
Example of reference activities and calculation of fingerprints for a magnet of standard size, with waiting time from 3 to 10 years.

Radionuclide	Reference activity (Bq/g) Waiting time: 3–10 years				Fingerprint (%)
	Copper	Steel	Iron	Whole magnet	Whole magnet
H-3	83.36	73.44	73.77	74.70	28.99%
C-14	0.01	0.01	0.01	0.01	0.004%
Na-22	0.10	0.51	0.29	0.29	0.11%
Cl-36	4.2E−04	0.01	0.00	1.6E−3	0.001%
Ar-39	0.24	12.72	0.55	1.74	0.67%
Ca-41	9.0E−04	3.2E−03	2.9E−03	2.7E−03	0.001%
Ti-44	0.37	1.75	1.54	1.44	0.56%
Mn-54	0.27	1.85	2.48	2.19	0.85%
Fe-55	17.57	136.67	191.10	168.30	65.32%
Co-60	33.92	7.60	0.32	4.41	1.71%
Ni-63	45.35	0.15	0.01	4.56	1.77%
Ag-108m	0.12	0.0E+00	1.1E−05	1.2E−02	0.004%

Table 6
Fingerprints for standard and small magnets, as a function of the waiting time.

Waiting time	Fingerprints (%)		
	Standard magnet		
	3–10 years	10–20 years	20–40 years
H-3	29.0%	62.0%	73.3%
C-14	0.004%	0.02%	0.04%
Na-22	0.1%	0.04%	0.002%
Cl-36	0.0006%	0.002%	0.006%
Ar-39	0.7%	2.3%	6.0%
Ca-41	0.001%	0.004%	0.01%
Ti-44	0.6%	1.8%	4.0%
Mn-54	0.9%	0.003%	n.a.
Fe-55	65.3%	26.2%	1.6%
Co-60	1.7%	1.9%	0.7%
Ni-63	1.8%	5.8%	14.2%
Ag-108m	0.004%	0.02%	0.04%
Total	100%	100%	100%

3.3. Fingerprints for the entire magnet

The nuclide vectors generated in different materials from the same irradiation scenario are directly comparable in the case of an electromagnet, because the different components are exposed to the same irradiation conditions (i.e., same irradiation and waiting time, same beam energy and similar position with respect to the beam).

It is therefore possible to establish one single fingerprint F_i for a magnet by combining the fingerprints $f_{i,j}$ of each material j via Eq. (3), where m_j is the mass fraction of the material j for a typical magnet. In the case of a magnet of the Super Proton Synchroton machine, which is representative of "standard" magnets with mass > 1 ton, the mass fractions are 10% copper, 80% iron and 10% stainless steel.

Calculation of fingerprints for the whole magnet from the reference specific activity of each material.

$$F_i = \sum_{j=1}^{3} m_j \times \frac{f_{i,j}}{\sum_l f_{l,j}} \qquad (3)$$

Table 5 presents an example of the application of Eq. (3) for the calculation of fingerprints in the case of such standard magnets. Table 6 present the fingerprints for standard magnets as a function of the waiting time.

4. Conversion factors and activity evaluation

A conversion factor CF (typically expressed in [Bq/g]/[μSv/h]) is a mathematical correlation between the specific activity contained in an object to be characterized and the measured dose-rate DR. For the purpose of the present study, it is useful to distinguish between a specific conversion factor cf_i, which applies to the dose-rate generated by the nuclide i alone, and a global conversion factor CF_i, which applies to the dose-rate generated by all the nuclides present in the magnet. The specific activity A_i of the radionuclide i can be calculated by means of Eq. (4), where F_i is the fingerprint of the radionuclide i as calculated with Eq. (3) and DR is the average value of dose-rate in contact with the magnet.

Use of conversion factors to convert the value of dose-rate into values of specific activity.

$$A_i = CF_i \times DR = \frac{F_i \times DR}{F_{\text{Ti-44}}/cf_{\text{Ti-44}} + F_{\text{Mn-54}}/cf_{\text{Mn-54}} + F_{\text{Co-60}}/cf_{\text{Co-60}}} \qquad (4)$$

The activity evaluation can be obtained by normalizing the global conversion factors presented in Table 7 with the dose-rate measured in contact with the magnet. These factors are obtained by applying Eq. (4) to the results provided in Table 6.

In Eq. (4) the sum in the denominator is limited to the three dominant gamma emitters, which together are responsible for over 95% of the dose-rate in the vicinity of the magnets. The next gamma emitter in order of importance is Na-22, although its production cross-section in stainless steel, iron and copper is much smaller than the one of Ti-44, Mn-54 and Co-60. Moreover, due to its relative short half-life (i.e., 2.6 years) with respect to Ti-44 (60 years) and Co-60 (5.6 years), its contribution to the dose-rate is bound to decrease exponentially with increasing waiting time.

A quantitative example of the contribution of Na-22 to the dose-rate is provided by the simulation with ActiWiz of the following activation scenario:

– activation within bulky materials surrounding the beam impact area;
– 20 years of irradiation;
– 3 years of waiting time (this is the shortest waiting time within the scope of this document and it maximizes the relative importance of Na-22).

The relative contribution of Na-22 to the ambient dose equivalent is then 1.8% for iron ARMCO, 2.1% for stainless steel 304L and 0.4% for copper OFE. Such small contribution will then further decrease with increasing waiting time.

The specific conversion factors of Ti-44, Mn-54 and Co-60 (i.e., 2.203, 5.86 and 1.81 (Bq/g)/(μSv/h) respectively) are taken from FLUKA simulations for stainless steel and copper slabs of 3 cm thickness, 100 cm length and 50 cm width. They are expressed as specific

Table 7
Global conversion factors to be used for activity evaluation.

| Waiting time | Global conversion factors (Bq/g)/(µSv/h) | | |
| | Standard magnet | | |
	3–10 years	10–20 years	20–40 years
H-3	21.6	33.3	32.7
C-14	0.003	0.01	0.02
Na-22	0.08	0.02	0.001
Cl-36	4.5E−04	0.001	0.003
Ar-39	0.5	1.2	2.7
Ca-41	0.001	0.002	0.004
Ti-44	0.4	0.9	1.8
Mn-54	0.6	0.002	n.a.
Fe-55	48.6	14.1	0.7
Co-60	1.3	1.0	0.3
Ni-63	1.3	3.1	6.3
Ag-108m	0.003	8.2E−03	0.02

activities normalized to one unit of dose rate in contact of the plate surface. Due to the phenomenon of self-shielding, the specific conversion factors at 3 cm thickness are more conservative than the ones for thicker slabs. On the other hand, considering a slab which is thinner than 3 cm would certainly lead to much higher conversion factors but would not be representative of the typical thickness of a magnet (i.e., in the range from 10–40 cm in the direction perpendicular to the beam).

The specific conversion factors are calculated for the case of a homogeneous activity distribution. However, in the case of magnets the activity is usually concentrated at the extremities near the beam line, leading to a non-homogeneous distribution. In particular, due to the way that secondary cascades build up, there is a gradient in activation which depends on the hadronic interaction length (typically > 10 cm) and ultimately on the beam energy. At the same time, it is virtually impossible to find isolated hotspots, where by "isolated hotspot" it is meant an area with concentrated activity and of radius smaller than the size of the detector chamber.

In order to demonstrate the absence of isolated hotspots, Fig. 1 shows the simulated distribution of dose-rate around a bending magnet irradiated in Super Proton Synchrotron complex. Due to the relatively high beam losses, the activity level of this magnet would be too high for elimination as TFA waste. Nevertheless, the activity distribution is representative of the one of less radioactive magnets. It is visible that the gradient in activation near the extremity and along the magnet itself is larger than the typical size of a detector chamber.

The establishment of the global conversion factors for the entire magnet relies on the assumption that all the three main parts (copper coils, iron yoke and steel supporting structure) are activated at the same time. This assumption is correct, in the sense that the secondary particles produced via nuclear interactions of a high-energy proton beam are very penetrating compared to the typical dimension of a magnet, as shown in Fig. 1. As an example, the global conversion factors for standard magnets are given in Table 7.

5. Overall characterization methodology

From an operational point of view, the characterization method is applied by determining a coarse radiological map of the magnet with dose-rate measurements using a 6150 AD6.[1] The measurement is performed with the device in contact of different magnet locations. Following this measurement step, an average dose-rate is calculated. Then, the conversion transfer function is applied to this average dose-rate to convert it into specific activities. From these specific activities the IRAS is calculated.

A limited number of dose-rate measurements is performed with the device in contact of each magnet following a well-defined procedure, which foresees the following measurement points:

---

(1) one point every 50 cm on the most active lateral face of the magnet;
(2) one point every 50 cm inside the magnet, if accessible;
(3) any identified hotspot inside and outside of the magnet;
(4) one point in both the front and rear faces of the magnet.

This way of performing measurements is very conservative because we focus on the most radioactive areas of the magnet (i.e. most radioactive lateral face, front faces and hotspot), which are not necessarily representative of the average level of specific activity especially for very large magnets.

Adding more measurements at representative locations would certainly lead to a more accurate estimate of the average dose-rate. An improvement of the accuracy of the average dose-rate would lead to less conservative values. Indeed, the greater the number of representative measurement points, the smaller the importance that is artificially attached to hotspots, and the more accurate the activity evaluation. At the same time, it is an ANDRA requirement that the characterization methodology remains "reasonably conservative" in order to reduce the risk of underestimating the activity.

6. Validation of the characterization method

In order to validate the characterization methodology, we select three magnets with IRAS > 1 using the transfer function characterization methodology (Fig. 2). These magnets are counted by gamma spectroscopy and the activity values are compared to the ones computed with the transfer function.

Characteristics of the magnets can be found in Table 8.

6.1. Comparison of gamma spectroscopy and transfer function results — local geometry

In order to validate the use of the transfer functions, we performed local gamma spectroscopy measurements with HPGe Falcon 5000 detectors[2] at two locations of the blue magnet where we previously measured the corresponding dose-rates. This type of measurement is important, as it is more consistent with assumptions of the transfer function method (semi-planar geometry).

6.1.1. Experimental setup

The measurement setup is shown in Fig. 4. An ISOCS (In Situ Object Counting Software) [12,13] model with a source that spans over the whole magnet volume is constructed to compute the efficiency curves. This method however presents some limitations of modeling but has the advantage to overcome the activity heterogeneity distribution inside the magnet. Figs. 3 and 4 respectively represent the ISOCS model used to compute efficiency curves and the experimental setup.

6.1.2. Results

Using the dose-rate at the location of the measurement, we compute activities of Na-22, Sc < Ti-44 and Co-60 using the transfer functions. Then, we compare these activity values with the ones obtained from the local gamma spectroscopy measurements. The results are summarized in Table 9.

We observe a relatively good agreement between the transfer functions and the local gamma spectroscopy measurement method, with a maximum ratio of 2.24. The local measurement is assumed with a uniform activity distribution inside the magnet. It should be noted that this hypothesis is also assumed for the derivation of the transfer functions method.

The agreement with the local gamma spectroscopy results corroborates that the transfer functions provide a valid method for calculating the referred three-radionuclide activities. It also indicates that the

---
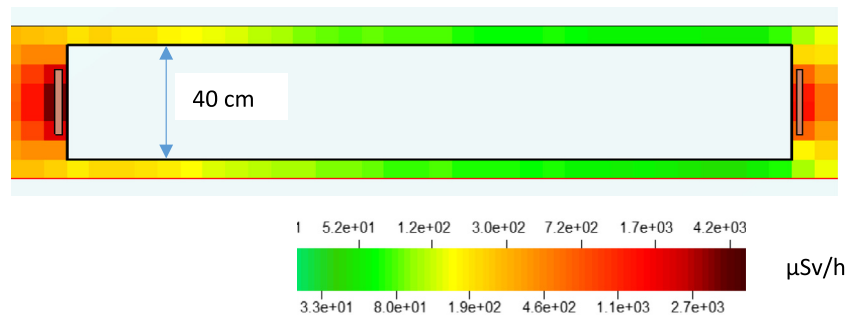
Fig. 1. Example of map of dose-rate around a magnet, as simulated with the Monte Carlo code Fluka. Top cross-sectional view of the magnet. This example reflects the dose rate distribution around a magnet but is not representative of the real dose-rate values expected in the magnets to be eliminated. (For interpretation of the references to color in this figure legend, the reader is referred to the web version of this article.)

Table 8
Main characteristics of magnets chosen for this study.

	Length (cm)	Width (cm)	Thickness (cm)	Material	Cooling time (years)	Weight (kg)	App. Density (g/cm3)	Av. Dose-rate (µSv/h)	Est. IRAS
Orange magnet	280	59.1	42.1	Standard	10–20 y	3870	5.55	58.3	14.27
Blue magnet	281.5	36	35	Standard	10–20 y	2650	7.47	13.4	3.27
Red magnet	250	137	110	Standard	3–10 y	24 000	6.37	7.8	2.42

Table 9
Comparison between local gamma spectroscopy measurements and transfer functions activity results where "HS" denotes hotspot.

	Dose-Rate (µSv/h)	Na-22 (Bq/g)	Sc < Ti-44 (Bq/g)	Co-60 (Bq/g)
HS1 g-spec	10.3	0.09	6.15	9.17
HS1 TRANS. FUNC.		0.21	9.27	10.30
Ratio HS1Func/H1g-spec	–	2.24	1.51	1.12

	Dose-Rate µSv/h	Na-22 Bq/g	Sc < Ti-44 Bq/g	Co-60 Bq/g
HS2 g-spec	3.93	0.04	2.15	3.40
HS2 TRANS. FUNC.		0.08	3.54	3.93
Ratio HS2Func/H2g-spec	–	2.06	1.65	1.16

transfer functions activity results are consistently conservative. Last but not least, it shows that the major source of conservativeness in the transfer function method comes indeed from the selection of measurement points for the computation of the average dose-rate, and not from assumptions made in the computation of the transfer functions themselves.

6.2. Comparison of gamma spectroscopy and transfer function results — global geometry

In order to validate the use of the transfer functions, we also performed integrated gamma spectroscopy measurements with High Purity Germanium Falcon 5000 detectors on the whole three magnets where we previously measured the corresponding dose-rates map. This type of measurement is important, as it allows direct comparisons with the transfer function method. However, as geometry model uncertainties can be quite high, we improved the spectroscopy results using the GURU tool [14] in order to quantify and optimize these uncertainties for the magnets. The tool makes use of the Canberra IUE (ISOCS Uncertainty Estimator). It allows quantifying the activity uncertainties (or the efficiency calibration uncertainties) due to the variation of the not-well-known geometry parameters. Based on a set of different geometry models that are generated by perturbing the geometry parameters in ISOCS, we perform a statistical analysis on the efficiency calibration and estimate the corresponding uncertainties. GURU goes one step further by performing the model optimization using the multi-count and line activity consistencies. Please refer to the paper [14] for more details about the used methodology. The best model corresponds to the

geometry model that provides the "closest" or consistent activity values in two opposite measurements or multi-line activities.

6.2.1. Experimental setup

We performed gamma spectroscopy measurements using the High Purity Germanium Falcon 5000 detectors.[3] The experimental setup is shown in Fig. 5. To ensure the whole magnet can be seen by the detector, the following measurements have been performed:

- On two large lateral faces where the detector pointed at the center of the face. The magnet-to-detector distance is half of the largest dimension of the face in order to optimize the coverage of the solid angle;
- On the two front faces of the magnets, in front of the vacuum chamber where the activity is typically the highest. Vacuum chambers are not always located at the middle of the side surface. Hence, the detectors are shifted to point at the center of the side-chamber openings. The magnet-to-detector distance is half of the largest dimension of the face, taking into account the shift.

The Figs. 5 and 6 respectively show the ISOCS geometry 3-D model used to compute efficiency curves and the experimental setup.

The gamma spectroscopy measurements on each detector are performed with a live time setting of 10,000 s.

6.2.2. Geometrical model uncertainties quantification

In a gamma spectroscopy report, activities are presented with their associated uncertainties. These uncertainties take into account the assumptions considered to compute the efficiency curves, the peak area and the emission probability. However, assumptions of the measurement geometry including the materials types and composition, the activity distribution, and dimensions are not included. In order to be able to compare gamma spectroscopy results with the transfer functions results, one has to quantify the discrepancy that can be generated by the not-well-known ISOCS model.

We first construct a reference model with ISOCS, referred to as M0 (Fig. 7). The M0 model is a complex box containing the radioactivity homogeneously distributed inside the magnet. The M0 ISOCS template complex box is presented in Fig. 8. The gamma spectroscopy measurements are often performed considering a uniform activity distribution

---

[3] http://www.gammadata.se/assets/Uploads/Falcon-SS-C38597.pdf.

Fig. 2. Magnets selected for the benchmarking of the characterization methodology. The magnets are referred to as "blue magnet", "orange magnet" and "red magnet" in the next sections of the document. (For interpretation of the references to color in this figure legend, the reader is referred to the web version of this article.)
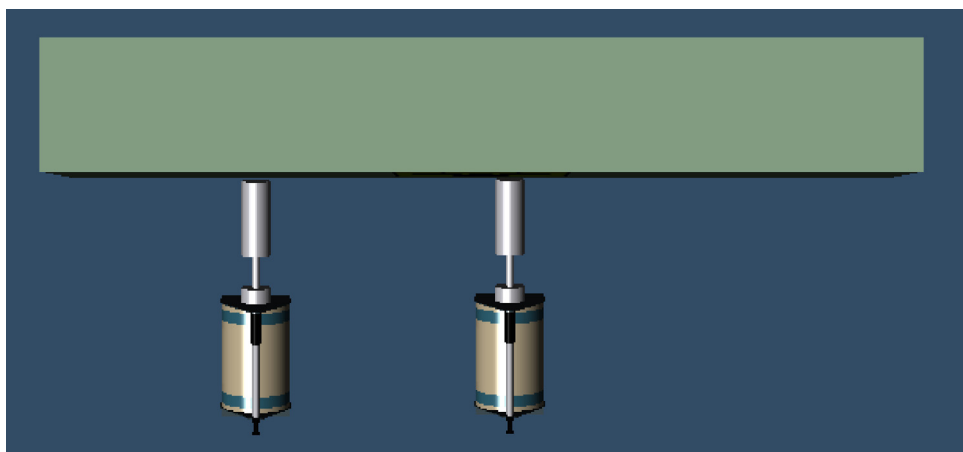

Fig. 3. ISOCS model of the experimental dispositive. Detectors are not modeled at the same time. Two independent measurements are performed.

Fig. 4. Local measurements on blue magnet. (For interpretation of the references to color in this figure legend, the reader is referred to the web version of this article.)
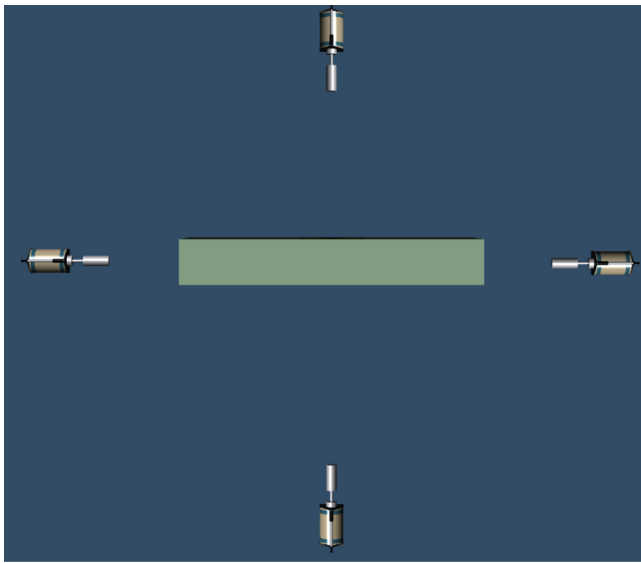

Fig. 5. ISOCS model of the experimental setup.

model in ISOCS for the efficiency calibration. However, in reality, the activation in an object is not uniform. As we cannot know the activity distribution within an object, we will perform the measurements with uniform activity distributions. The objective is to estimate the error induced by the uniform model. Hence, the reference model (model 0) is uniform, considering only one layer in the complex box template.

Since the activity distribution within the magnets is unknown, a uniform activity distribution is assumed. Moreover, in order to optimize the detector coverage via the solid angle, the magnet-to-detector distance is selected to be half of the largest dimension of the measurement face (Fig. 7).

In the M0 models we define the reference values for the hotspot concentrations, as well as the characteristic dimensions of the magnets. We perturb these values using Isocs Uncertainty Estimator (IUE) to study the impact of the variation of geometry parameters on the efficiency curve uncertainties. The variable parameters are sampled using a uniform distribution within their corresponding intervals. It is worth noting that a positive perturbation of the efficiency curve leads to a negative perturbation of the activity, following Eq. (5) below: Activity

calculation by gamma spectroscopy.

$$A = \frac{N_s(E)}{\varepsilon(E).\Delta t} \times \frac{1}{I_\gamma(E)} \tag{5}$$

where:

A is the activity of a certain radionuclide in the decay series;

$N_s(E)$ is the net peak area corresponding to energy E;

$\varepsilon(E)$ is the absolute efficiency corresponding to the geometric model at energy E;

$I_\gamma(E)$ is the emission intensity of photons with energy E (full energy peak);

Δt is time for collecting the spectrum of the sample.

Consequently we perform perturbations for all possible parameters in the best-known probable variation range. In total approximatively 2000 ISOCS models for both the detector front and side positions have been generated. The perturbed parameters are the following:

- Material considered relies on different combinations of the three base material compositions described in Table 1. The modeled combinations are respectively for IRON_ARMCO, STEEL_304L and COPPER_CUOFE: 100/0/0%, 0/100/0%, 80/10/10%, 70/20/10%;
- Hotspot locations in the entire magnet;
- Hotspot dimensions in the entire magnet;
- Relative hotspot concentrations (from 0.1 to 15);
- Number of hotspots (from 1 to 10).

The efficiency uncertainties are presented in Fig. 9 for the front face detectors. The range of variations are similar for side detectors. We first observe that the average efficiency values are approximatively 40% lower compared to M0. This shows that presence of hotspots lowers the efficiency by a factor of approximately 2 compared to a homogeneous activity distribution. Hence, the resulting activities are underestimated by a factor of ∼2. Most of the calculation results (average + 1 standard deviation) give efficiency values ranging from −60% and −20% compared to the homogeneous case (M0). However, for some cases, the efficiency can be perturbed in the area of −90% +180% resulting in an activity value being potentially divided by 2 or multiplied by 10. In the case of magnets, the higher perturbations of efficiency calibration originate from the activity distribution heterogeneity (hotspots) as it is already observed in [15].

For this reason, the next part of this document targets the identification of the actual activity distribution within the magnets.

6.2.3. Efficiency of the optimization method with magnets

The 2000 models previously generated with the geometry perturbations are used for the optimization process. The optimization is performed using the two pairs of lateral and front measurements independently. The multi-count and line activity consistencies are performed by GURU on these 2000 models to find a set of "best models", first on the two lateral measurements and then on the two front measurements. A "best model" fulfills the conditions that two opposite faces should have the same activity. The activity optimization results are summarized in Fig. 10.

We can see that the optimization is successful for almost all the radionuclides in all the magnet types except for two cases:

- For the blue magnet with detectors located in front of the lateral faces, the ratio between the two detectors for Sc < Ti-44 is around 0.2 after optimization whereas it was 0.04 before optimization.

Fig. 6. Global measurements on blue magnet. (For interpretation of the references to color in this figure legend, the reader is referred to the web version of this article.)
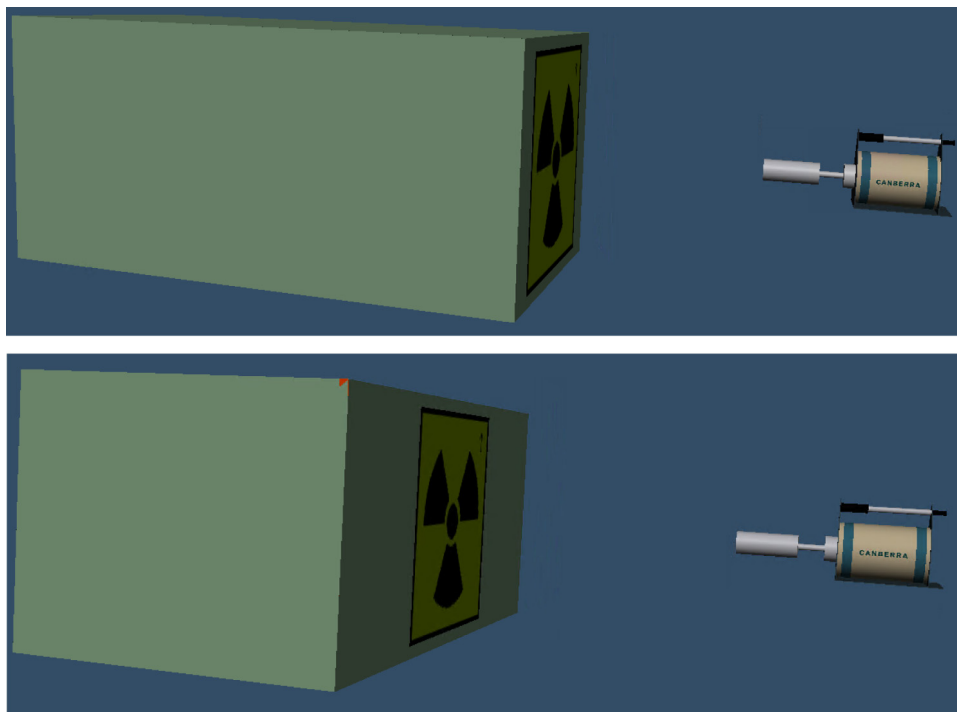

Fig. 7. ISOCS 3-D geometry of the red magnet for parameter perturbations representing the reference calculation with measurements of the front face and lateral face.

The ratio is improved but is not reaching a value close to 1. We think this is due to the limitation of the models considered during the optimization process. It means that the database of various efficiency curves used to optimize the activity results does not contain a ''best model'' that is of sufficient quality to allow for good convergence of the optimization.
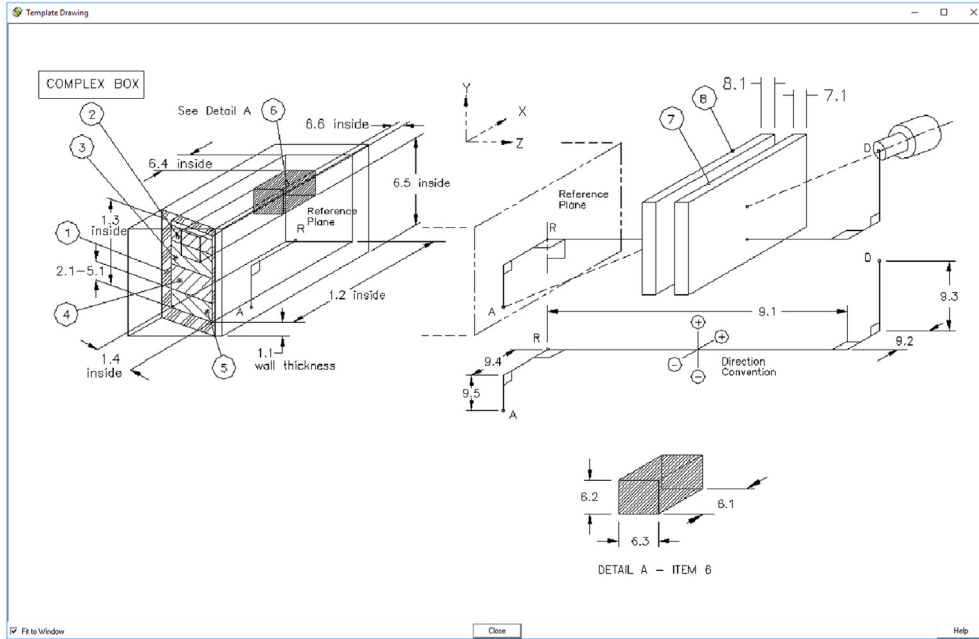
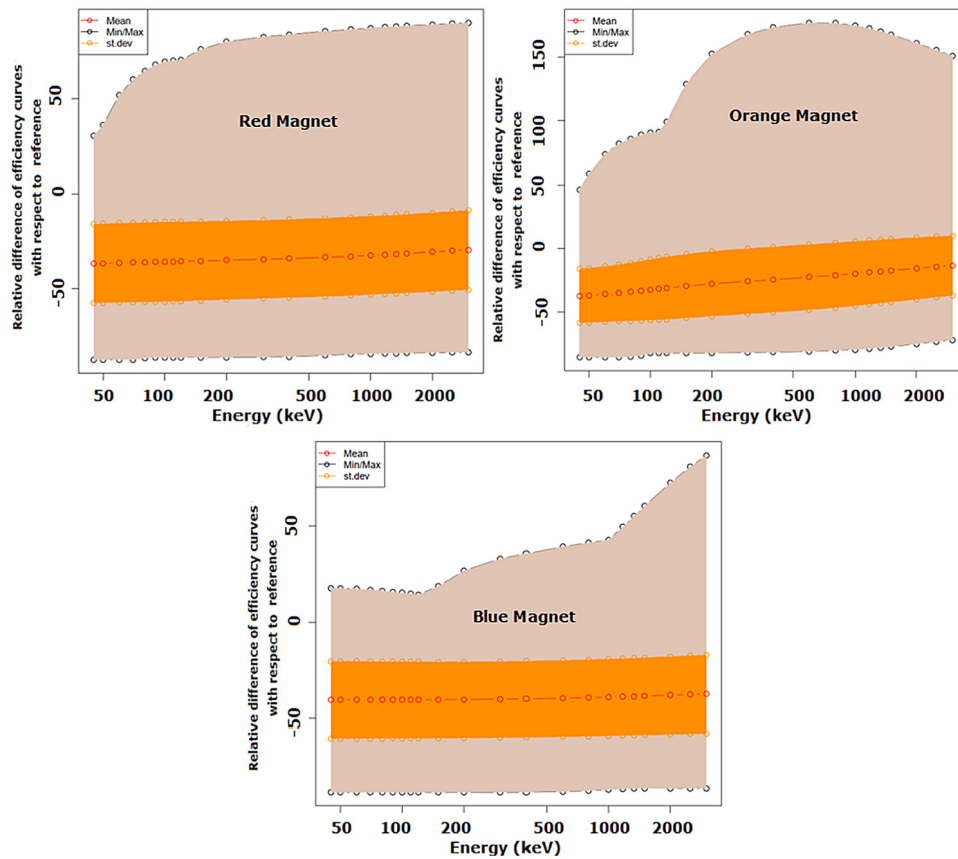**Fig. 8.** ISOCS complex box template used to model the magnets.

Fig. 9. Relative difference (%) between efficiencies from perturbed models and from the reference model. The red curve shows the average of all the efficiencies, the orange part is the range of variation at 1σ and the gray part describes the complete range of variation. (For interpretation of the references to color in this figure legend, the reader is referred to the web version of this article.)

Table 10

Comparisons between opposite measurements activities for each front and lateral configuration and the three magnets before and after optimization of the assumed spatial activity distribution. Activities are given in units of Bq/g for the gamma radionuclides of interest. Uncertainties are given at 2 sigma and include the counting, nuclear data, peak fitting, intrinsic ISOCS and the ISOCS geometry uncertainties. We see that before optimization, the uncertainty is driven by the geometry, around 70% at 2 σ.

Orange magnet		Before optimization		After optimization	
		Detector 1	Detector 2	Detector 1	Detector 2
Front faces	Na-22	0.13 (70.7%)	0.15 (71.2%)	0.19 (27.0%)	0.19 (28.1%)
	Sc < Ti-44	5.53 (70.5%)	9.66 (70.7%)	8.54 (26.2%)	8.54 (26.9%)
	Co-60	8.27 (70.4%)	8.27 (70.7%)	10.32 (26.1%)	10.31 (26.9%)
Lateral faces	Na-22	0.01 (73.0%)	0.02 (77.7%)	0.02 (42%)	0.02 (32.5%)
	Sc < Ti-44	2.66 (70.8%)	8.62 (70.9%)	7.16 (27.4%)	7.14 (27.0%)
	Co-60	2.85 (70.7%)	2.81 (70.7%)	2.66 (26.9%)	2.62 (26.9%)

Blue magnet		Before optimization		After optimization	
		Detector 1	Detector 2	Detector 1	Detector 2
Front faces	Na-22	0.05 (73.1%)	0.08 (71.5%)	0.13 (32.8%)	0.13 (29.0%)
	Sc < Ti-44	1.32 (70.9%)	3.44 (70.8%)	2.84 (27.4%)	2.84 (27.2%)
	Co-60	8.23 (70.7%)	8.70 (70.7%)	13.00 (26.9%)	13.00 (26.9%)
	Ag-108m	0.10 (71.2%)	0.16 (71.1%)	0.17 (28.2%)	0.17 (28.0%)
Lateral faces	Sc < Ti-44	3.16 (71.3%)	0.14 (70.9%)	1.15 (28.5%)	0.23 (27.4%)
	Co-60	4.00 (70.8%)	0.47 (70.7%)	2.16 (27.0%)	1.63 (26.9%)

Red magnet		Before optimization		After optimization	
		Detector 1	Detector 2	Detector 1	Detector 2
Front faces	Na-22	0.03 (71.8%)	0.30 (71.1%)	0.17 (29.6%)	0.21 (28.0%)
	Sc < Ti-44	0.23 (71.1%)	0.56 (71.0%)	0.25 (28.0%)	0.27 (27.7%)
	Co-60	1.69 (70.7%)	9.23 (70.7%)	8.90 (26.9%)	8.83 (26.9%)
	Ag-108m	0.01 (76.0%)	0.02 (73.6%)	0.01 (45.0%)	0.01 (29.7%)
	Mn-54	0.03 (79.4%)	0.29 (71.8%)	0.03 (38.7%)	0.10 (33.8%)
Lateral faces	Sc < Ti-44	0.13 (71.4%)	0.02 (72.5%)	0.17 (28.7%)	0.17 (31.3%)
	Co-60	1.66 (70.7%)	1.67 (70.7%)	1.38 (26.9%)	1.38 (27.0%)
	Mn-54	0.45 (71.7%)	0.02 (75.3%)	0.23 (29.5%)	0.22 (37.3%)

Table 11

Activity results comparison before and after optimization. Activities are given in units of Bq/g for the gamma radionuclides of interest. Standard deviation of the mean allows to quantify the discrepancy between two opposite measurements before and after optimization. Uncertainties are given at 2 σ.

Orange magnet				
Radionuclide	Before optimization		After optimization	
	Average	Std of the mean between measurements	Average	Std of the mean between measurements
Na-22	0.08 (71.5%)	46%	0.10 (28.0%)	49%
Sc < Ti-44	6.57 (70.7%)	13%	7.85 (26.8%)	3%
Co-60	5.51 (70.6%)	19%	6.48 (26.6%)	22%
Ag-108m	6.02E−02 (71.0%)	No meaning	–	–

Blue magnet				
Radionuclide	Before optimization		After optimization	
	Average	Std of the mean between measurements	Average	Std of the mean between measurements
Na-22	0.06 (72.1%)	23%	0.13 (30.9%)	<0.1%
Sc < Ti-44	1.99 (71.0%)	23%	1.77 (27.5%)	16%
Co-60	5.3 (70.7%)	24%	7.45 (26.9%)	28%
Ag-108m	0.13 (71.1%)	11%	0.17 (28.1%)	2%

Red magnet				
Radionuclide	Before optimization		After optimization	
	Average	Std of the mean between measurements	Average	Std of the mean between measurements
Na-22	0.15 (71.2%)	80%	0.19 (28.7%)	11%
Sc < Ti-44	0.24 (71.1%)	38.31%	0.23 (28.7%)	9%
Mn-54	0.20 (72.1%)	35%	0.15 (33.7%)	28%
Co-60	3.54 (70.7%)	21%	5.12 (26.9%)	5%
Ag-108m	1.1E−02 (74.4%)	54%	1.0E−02 (37.4%)	33%

- In the case of Mn-54 and the red magnet with detectors located at the front faces, we see that the ratio after optimization is around 3 whereas it was 11 before optimization. The ratio is improved but is not reaching a value close to 1, for probably the same reason as described above.

For all the other cases, the optimization gives activity ratios consistent with unity, even when they were above a factor of 2 before optimization, showing a successful optimization methodology.

However, the optimization is performed sequentially, first on the two detectors positioned at the front faces and then on the two lateral faces, losing some constraints compared to a 4-detector optimization.

Table 10 illustrates these discrepancies between measurements at the lateral and front faces.

We find discrepancies between activities measured at the magnet's front and at its lateral faces of:

- A factor of 5 for Co-60,
- A factor of 2 for Sc < Ti-44,
- A factor of 8 for Mn-54,
- A factor of 10 for Na-22.

It should be noted that Na-22 is a radionuclide typically found in aluminum. The fact that the presence of aluminum varies considerably between front and lateral faces can originate from the high heterogeneity of its activity distribution.

These discrepancies will obviously have an impact on the global activity uncertainty after optimization but the activity bias (described in Section 6) will be correctly taken into account. The four gamma spectroscopy results are averaged to estimate the activity of each magnet after optimization.

6.2.4. Reconstruction of average activity over the magnet

In Table 11 we present the activities obtained by gamma spectroscopy before and after optimization. The standard deviation between the four detectors results is also provided in this table.

We observe in Table 11 that all activities are corrected by a factor close to the observed bias of approximatively 40%, presented in the previous Section 6.2.2. Moreover, most of the standard errors related to the four detector averages are reduced except for Na-22 and Co-60 in the orange magnet, and Co-60 in the blue magnet. This originates from the fact that the implemented method optimizes first the activities on the two front faces detectors, and then on the two lateral faces detectors, leading to discrepancies between the four measurements. In all cases, except for Ag-108m and Sc < Ti-44 in the red magnet, the activity values are increased after optimization, as predicted in Fig. 9.

6.2.5. Comparison of gamma spectroscopy "best model" with transfer functions

In order to observe how the optimization of gamma spectroscopy impacts the ratio measurement/transfer function, Table 12 details the comparison results. Based on the technical specification of the AD6 measurement device,[4] the dose linearity has a maximum deviation of ±10% and the energy response ranges from between −30% and +30%. Hence, we assume a measurement uncertainty of 20% at 2 σ.

The results in Table 12 show that, in general, optimized modeling of the spatial activity distribution allows for reducing the ratio between the transfer function and the gamma spectroscopy activity estimations. Hence, the transfer functions methodology allows for a robust computation of the activities. In particular, the transfer function methodology consistently overestimates the activities compared to

---

[4] http://www.radtech.it/Data/Sites/1/media/documents/products/Prospekt_6150AD_E.PDF.
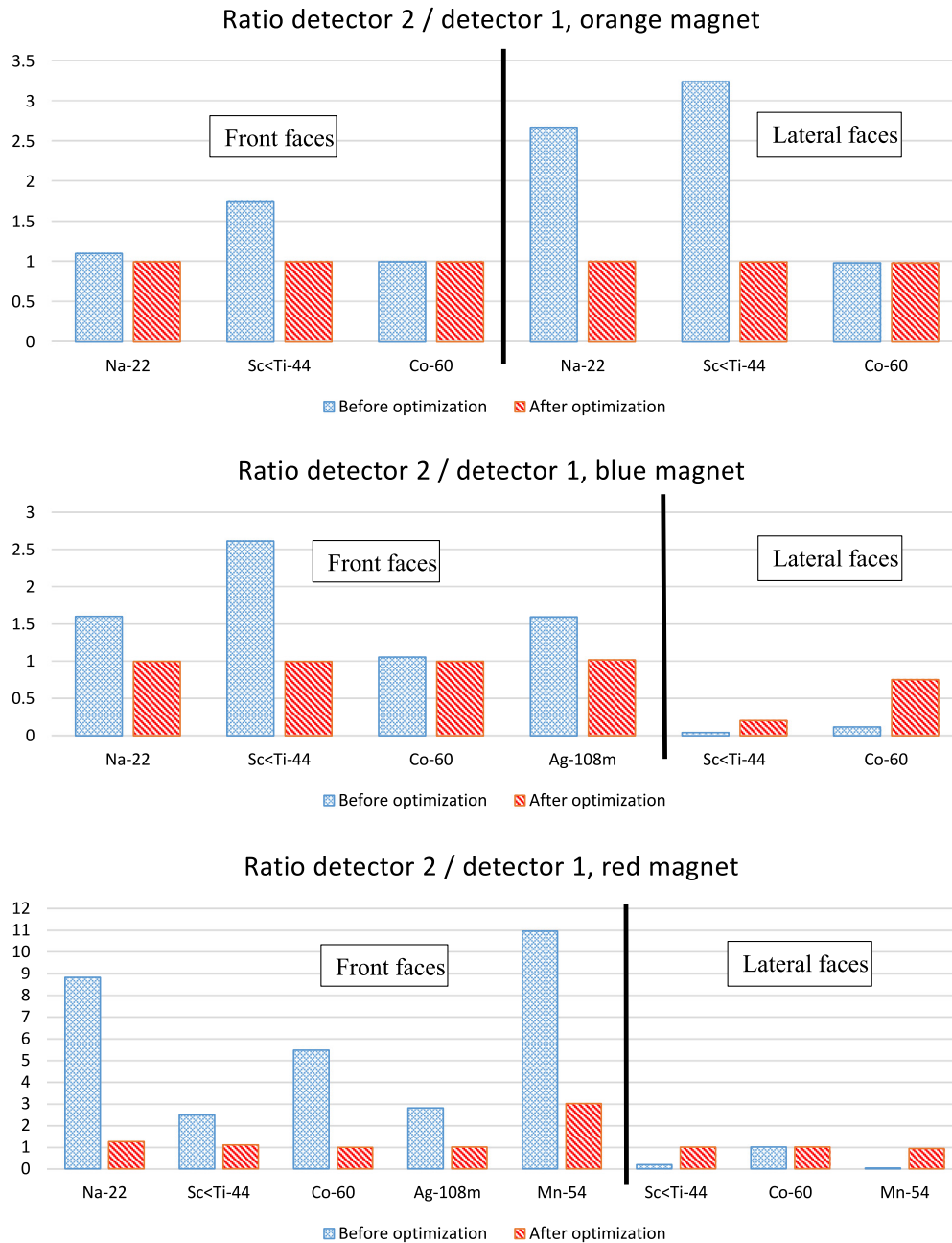
Fig. 10. Ratio between opposite measurements activities for each front and lateral configuration and the three magnets. A ratio close to 1 shows that a model of the spatial activity distribution could be identified that better describes the real situation rather than a homogeneous distribution.

gamma spectroscopy. Finally, we draw the attention of the reader to the following points:

- For Ag-108m, in the orange magnet, it is not possible to perform the model optimization due to the absence of this nuclide in three of the four gamma spectroscopy measurements.
- For Ag-108m in the blue magnet, the activity ratio of the transfer function and gamma spectroscopy after optimization is below 1. However, only two gamma spectroscopy measurements of the four have an activity above the MDA (Minimum Detectable Activity). Consequently, the average activity is overestimated as activity values below the MDA are considered as 0.
- Finally, with the red magnet, we observe an increase of the ratio after optimization for Sc < Ti-44, Mn-54 and Ag-108m, for the same reason explained previously.

Furthermore, as a general conclusion of this section, even after excluding the dose-rate measurement values of the hotspots and inside the magnet, the transfer function remains conservative. Hence, these dose-rate measurements could be excluded without introducing a significant risk of underestimating the activity.

7. Conclusions

This paper describes a characterization methodology, which allows the establishment of a complete radionuclide inventory (including difficult-to-measure radionuclides) with conservative estimates of specific activity by means of a simple dose-rate survey, without resorting to in-situ gamma spectroscopy, dedicated Monte Carlo simulations or destructive analysis. In the case of electromagnets at CERN, this method does not require precise knowledge of the radiological history, material composition or position in the proton machine during irradiation.

Fig. 11. Elimination of first electro-magnets as unitary pieces. Left figure: handling of magnet on the truck. Right figure: elimination in ANDRA's repository. Courtesy of ANDRA.

Table 12
Comparisons of the activity assessments originating from gamma spectroscopy with the best optimized model and standard model as well as the transfer function method for the three magnets. Uncertainties are given at 2 σ.

Radionuclide	Ratio between average activity Transf. function and standard gamma spectroscopy results	Ratio between average activity Transf. function and improved gamma spectroscopy results	Ratio between average activity Transf. function and standard gamma spectroscopy results	Ratio between average activity Transf. function and improved gamma spectroscopy results
	Including all dose-rate measurements		Without internal and hotspot dose-rate measurements	
Orange magnet				
Na-22	15.0 (74.2%)	11.8 (34.4%)	3.8 (74.2%)	2.9 (34.4%)
Sc < Ti-44	8.0 (73.5%)	6.7 (33.5%)	2.2 (73.5%)	1.9 (33.5%)
Co-60	10.6 (73.4%)	9.0 (33.3%)	3.0 (73.4%)	2.5 (33.3%)
Ag-108m	10.0 (73.9%)	–	2.7 (73.9%)	–
Blue magnet				
Na-22	5.0 (74.8%)	2.3 (36.8%)	3.3 (74.8%)	1.5 (36.8%)
Sc < Ti-44	6.0 (73.8%)	5.2 (34.0%)	5.6 (73.8%)	4.9 (34.0%)
Co-60	2.5 (73.5%)	1.8 (33.5%)	2.3 (73.5%)	1.7 (33.5%)
Ag-108m	1.0 (73.9%)	0.8 (34.5%)	0.9 (73.9%)	0.7 (34.5%)
Red magnet				
Na-22	4.7 (73.9%)	3.6 (35.0%)	2.7 (73.9%)	2.1 (35.0%)
Sc < Ti-44	14.2 (73.9%)	14.9 (35.0%)	8.3 (73.9%)	8.8 (35.0%)
Mn-54	25.0 (74.8%)	33.9 (39.2%)	14.5 (74.8%)	19.7 (39.2%)
Co-60	3.1 (73.5%)	2.1 (33.5%)	1.8 (73.5%)	1.3 (33.5%)
Ag-108m	2.5 (77.0%)	3.8 (42.4%)	1.5 (77.0%)	2.2 (42.4%)

In order to obtain the list of relevant radionuclides, systematic calculations with the code ActiWiz are performed to study the activation scenarios which can lead to induced radioactivity in magnets from the CERN proton machines.

The fingerprints for the different types of magnets are then established as a function of the waiting time. The evaluation of absolute levels of specific activity is obtained by normalizing the average dose-rate in contact with a magnet, using global conversion factors, which allows for the characterization of CERN's electromagnets without recurring to any gamma spectroscopy measurement.

We have shown in this document that the transfer function method represents a reliable and robust technique for the evaluation of specific activity in the case of magnets with very-low-level activity, as long as we select dose-rate measurement points which are sufficiently representative of the activity distribution in the magnet. This is particularly true for the dominant gamma emitters (Na-22, Ti-44 and Co-60). The matching between transfer functions and in-situ gamma spectroscopy is even

more satisfactory once the models used in the analysis are improved following the methodology described in the previous sections.

The values obtained with the transfer functions are reasonably conservative when we measure the dose-rate at the front faces and on the most radioactive lateral face (i.e., they are conservative by a factor of ~3). The values become extremely conservative (i.e., by a factor of ~10) when we include the dose-rate measurements inside the magnets (internal) and at the hotspots, as foreseen in the current measurement procedure.

The reasons why the activity evaluation can be very conservative are:

– The transfer functions are designed for contact dose-rate measurements of a planar surface, but would lead to activity overestimation if applied to full-immersion measurements (as is the case inside of a magnet);
– In the current operational procedure adopted at CERN, the hotspot is counted twice for the calculation of the average dose-rate;
– Only the dose rate of the most radioactive lateral face is measured.

Overestimating the activity of the dominant gamma emitters by a factor of 10 can lead to comparable overestimation of the IRAS factor. It is therefore important to optimize the procedure for the selection of measurement points considered in the dose-rate survey.

All in all, this validation study confirms the validity of the transfer functions method when applied to electromagnets at CERN.

Due to the limitation in IUE to perform efficiency model perturbations on the four detectors simultaneously (on the two front and two lateral faces), we recommend investigating the development of a new tool in a future version of GURU, which would allow for computing the efficiency curves without the intermediate IUE step. This could be achieved for example by calling the ISOCS program in a batch mode with GURU software processes.

The characterization method presented is currently used at CERN for the elimination of electromagnets towards the French repository managed by ANDRA (Fig. 11). We believe that the overall methodology, including the algorithms for the identification of relevant radionuclides and the establishment of fingerprints and transfer functions, as well as the optimization of gamma spectroscopy measurements, can be applied to other cases of very low-level waste produced in other research institutes using high energy particle accelerators.

Declaration of competing interest

The authors declare that they have no known competing financial interests or personal relationships that could have appeared to influence the work reported in this paper.

References

[1] R. Froeschl, C. Theis, F. La Torre, H. Vincke, N. Walter, S. Sgobba, Radiological Hazard Classification of material in CERN's accelerators. ERN-DGS-2012-003-RP-IR, EDMS. ID: 1184236, Geneva.

[2] B. Zaffora, M. Magistris, G. Saporta, J.-P. Chevalier, Uncertainty quantification applied to the radiological characterization of radioactive waste, Appl. Radiat. Isot. 127 (2017) 142–149.

[3] K. Delbeke, H.P. Rodrigez, Copper Concentrates, Technical report, European Copper Institute, 2014.

[4] H. Vincke, C. Theis, Actiwiz - optimizing your nuclide inventory at proton accelerators with a computer code, in: ICRS12 Conference, 2012.

[5] Ferrari, et al., FLUKA: A Multi-Particle Transport Code, CERN-2005-10, 2005.

[6] G. Battistoni, et al., The fluka code: description and benchmarking, in: Hadronic Shower Simulation Workshop, Fermilab, 2006.

[7] B. Zaffora, et al., A new approach to characterize very-low-level radioactive waste produced at hadron accelerators, Appl. Radiat. Isot. 122 (2017) 141–147.

[8] IAEA, Strategy and Methodology for Radioactive Waste Characterization, IAEA-TECDOC-1537, Vienna, 2007.

[9] IAEA, No. NW-T-1.18. Determination and Use of Scaling Factors for Waste Characterization in Nuclear Power Plants, IAEA, Vienna, 2009.

[10] ISO 16966, Nuclear Energy - Nuclear Fuel Technology - Theoretical Activation Calculation Method To Evaluate the Radioactivity of Activated Waste Generated At Nuclear Reactors, International Standard Organization, Geneva, 2013.

[11] ISO 21238, Nuclear Energy - Nuclear Fuel Technology - Scaling Factor Method To Determine the Radioactivity of Low- and Intermediate-Level Radioactive Waste Packages Generated At Nuclear Power Plants, International Standard Organization, Geneva, 2007.

[12] F. Bronson, B.M. Young, V. Atrashkevich, ISOCS mathematical Calibration software for germanium gamma spectroscopy of small and large objects, in: Transactions of the American Nuclear Society Annual Meeting, 1997.

[13] R. Venkataraman, F. Bronson, V. Atrashkevich, M. Field, B.M. Young, Improved detector response characterization method in ISOCS and labsocs, in: Methods and Applications of Radioanalytical Chemistry (MARC VI) Conference, 2003.

[14] T. Frosio, C. Theis, A novel technique for the optimization and reduction of gamma spectroscopy geometry uncertainties. https://doi.org/10.1016/j.apradiso.2019.108953.

[15] T. Frosio, N. Menaa, C. Duchemin, N. Riggaz, C. Theis, A new gamma spectroscopy methodology based on probabilistic uncertainty estimation and conservative approach, Appl. Radiat. Isot. 155 (2020).